Sign reversal of the Hall effect in the flux flow region of $Bi_{2+x}Sr_{2-x}CuO_{6+\delta}$

Qihao Zang,[1] Zuyu Xu,[2] Huiqian Luo,[3] Hua-Bing Wang,[2,4] and Hai-Hu Wen[1,*]

[1]*National Laboratory of Solid State Microstructures and Department of Physics, Collaborative Innovation Center of Advanced Microstructures, Nanjing University, Nanjing 210093, China*

[2]*Research Institute of Superconductor Electronics, Nanjing University, 210093 Nanjing, China*

[3]*Beijing National Laboratory for Condensed Matter Physics, Institute of Physics, Chinese Academy of Sciences, Beijing 100190, China*

[4]*Purple Mountain Laboratories, Nanjing 211111, China*

(Received 5 January 2024; revised 6 March 2024; accepted 12 April 2024; published 2 May 2024)

We have measured the longitudinal and transverse resistivity, ρ_{xx} and ρ_{xy} on the optimally doped $Bi_{2+x}Sr_{2-x}CuO_{6+\delta}$ single crystals with a well-shaped Hall bar structure. It is found that the Hall resistance in the flux flow region exhibits a clear sign-reversal effect. The strongest reversal Hall signal appears in the region of about the half-transition way, either on the temperature dependence of ρ_{xy} at a fixed field or the field dependence of ρ_{xy} at a fixed temperature. Detailed analysis shows that the theoretically proposed scaling law $\rho_{xy} = A\rho_{xx}^{\beta}$ with $1.5 < \beta < 2$ in the small dissipation limit is not obeyed very well. The Hall resistivity is plotted in a $H - T$ phase diagram, and the boundary for the Hall reversal effect to occur follows the theoretical prediction of Feigel'man *et al.* [JETP Lett. **62**, 834 (1995)], which suggests that the anomalous Hall effect may be induced by the properties of a single vortex, rather than by the collective flux motion with pinning and strong thermal fluctuations.

DOI: 10.1103/PhysRevB.109.174501

I. INTRODUCTION

In many type-II superconductors, the Hall resistance changes its sign when it enters the flux flow region, which has been termed the anomalous Hall effect (AHE) in superconductors. The AHE has been observed in most of the high-T_c cuprate superconductors, such as $Bi_2Sr_2CaCu_2O_8$ (BSCCO) [1,2], $Tl_2Ba_2CaCu_2O_8$ (TBCCO) [3–5], $Tl_2Ba_2Ca_2Cu_3O_{10-\delta}$ [6], $YBa_2Cu_3O_{7-\delta}$ (YBCO) [7–13], and $HgBa_2CaCu_2O_{6+\delta}$ [14]. Remarkably, it was claimed that the AHE usually appears only in underdoped cuprate superconductors, but not in the overdoped regions [15], although no further data can be found to support this statement. The AHE has also been observed in some conventional superconductors [16–18] as well as in iron-based superconductors [19,20]. Clearly, the traditional Bardeen-Stephen theory [21] cannot explain the AHE, since this theory leads to the conclusion that the Hall resistivity in the mixed state and the normal state should have the same sign. Although several theoretical models have been proposed to explain this AHE, the mechanism for AHE remains still elusive.

For the vortex motion involved with the AHE, it is very important [3,22,23] to know whether the Magnus force exists or not. Friedel *et al.* put forward the argument for the existence of Magnus force [24]. In 1966, Nozières and Vinen [25] proved the existence of magnus force acting on a vortex line. Later, the Magnus force acting on the vortex line was proved to exist universally in describing the vortex motion of type-II superconductors [26]. However, we should note that the Magnus force alone will not lead to the AHE. There have been several theoretical models for explaining the origin of the AHE. Most of them started from the basic equations of vortex motion, namely, the Lorentz force is equated with the dissipative force and the Magnus force, and other terms including the quenched disorders (pinning effect), interaction between vortex lines, and the thermal noise. Thus, different inclusions or emphasis would lead to diverse conclusions about the AHE from different groups. Wang *et al.* treated the problem based on the Bardeen-Stephen approach, considering the backflow effect, the pinning effect, and thermal fluctuations. They concluded that the pinning is very crucial in determining the AHE [27,28]. However, Vinokur *et al.* thought that the AHE is independent of the pinning [29], and both topological contribution and normal excitation should be taken into account, thus attributed the AHE to the imbalanced excess charge in the vortex core region [30]. Other models attributed the AHE to superconducting fluctuations [31–33], vacancies or dislocations in a pinned vortex lattice [34], Berry phase [26], and unusual Seebeck effect [35,36]. Furthermore, experimentally, a puzzling scaling behavior, $\rho_{xy} = A\rho_{xx}^{\beta}$ with $1.5 < \beta < 2$, has been observed in some cuprate superconductors [2,5,11,13,37] with the AHE. However, concerning the origin and determining factors for the AHE, it has not reached a consensus yet.

In this paper, we report the measurements of the longitudinal and Hall resistivity on a Hall bar of the $Bi_{2+x}Sr_{2-x}CuO_{6+\delta}$ ($x = 0.05$, $T_c^{zero} \approx 6.7$ K) single crystal, which is close to the optimal doping level in this system [38]. We observed a pronounced signal of sign reversal of the Hall resistance in the Bi2201 sample in the flux flow region. We also depicted the phase diagram of the Hall resistivity and determined the

*hhwen@nju.edu.cn

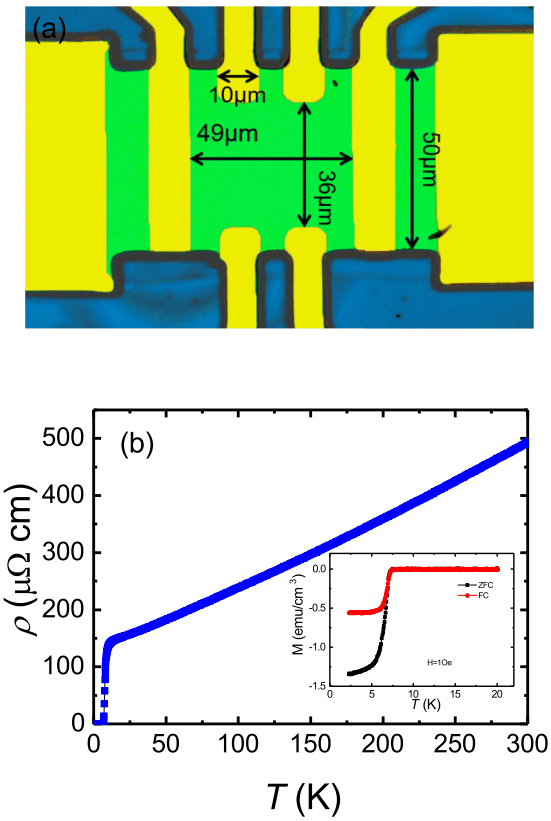

FIG. 1. (a) Optical image of our Bi2201 Hall bar (with modifications of colors for different regions). The green area in the middle denotes the Bi2201 sample. The yellow areas represent the gold electrodes. The sizes of the Bi2201 sample and gold electrodes are also displayed by arrowed lines. (b) Resistivity as a function of temperature for the Bi2201 sample. The inset in (b) displays the magnetization as a function of temperature measured under 1 Oe.

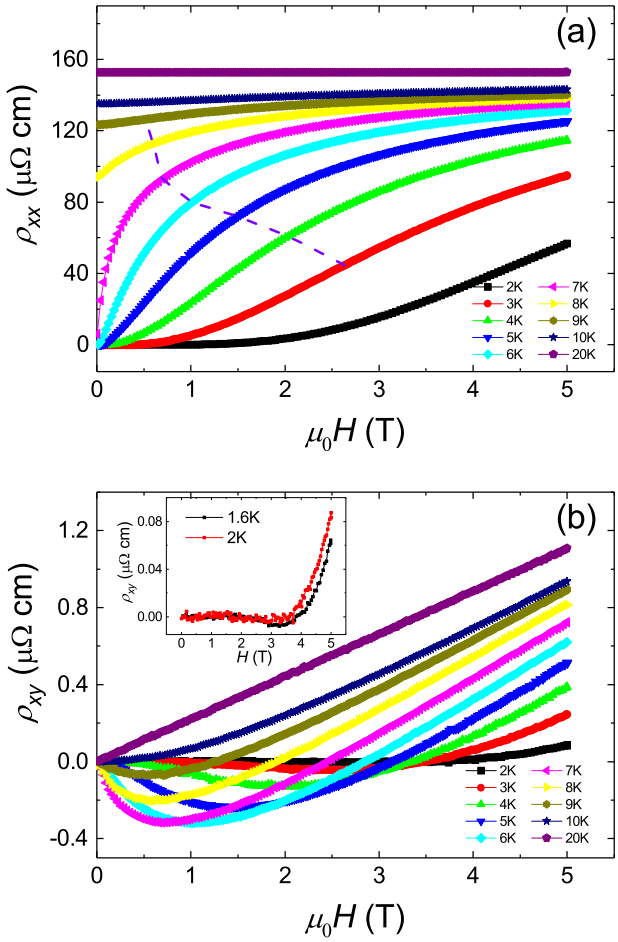

FIG. 2. (a) Longitudinal resistivity of the Bi2201 sample as a function of magnetic field at different temperatures. The dark purple dashed line denotes the positions of the maximum negative Hall resistivity in Fig. 2(b). (b) Hall resistivity of Bi2201 as a function of magnetic field at different temperatures. Above 10 K, there is no sign reversal in the Hall resistivity. Below 9 K, negative Hall resistivity begins to appear. The inset in (b) shows the Hall resistivity at 1.6 K and 2 K.

boundary for the AHE to occur. We adopted the theoretical expressions given by the model of Feigel'man *et al.* [30] to analyze the data. Our results are in good agreement with theoretical expectations [30].

II. EXPERIMENTAL RESULTS

A. Hall resistance sign reversal

The sample was grown by using the traveling solvent floating zone technique [38]. The bridge used here is the same one used for the high-field transport measurements, and the fabrication process of our Bi2201 Hall bar was described in that study [39]. The measurements of resistivity and Hall resistivity are carried out with a physical property measurement system (PPMS, Quantum Design). Figure 1(a) displays the optical image (with modified colors for different areas) of our Bi2201 Hall bar. In Fig. 1(a), the yellow areas denote the gold electrodes, and the wider electrodes on both sides are current electrodes. The green area represents the body of the Bi2201 sample for the transport measurements. The sizes of the Bi2201 sample and gold electrodes are also displayed in Fig. 1(a). Using an atomic force microscope (AFM), we measured the thickness of the sample, which is about 1.5 μm. Using these sizes, we can more precisely get the related longitudinal resistivity, Hall resistivity and Hall conductivity. Figure 1(b) displays the resistivity as a function of temperature for the Bi2201 sample at zero field, and the zero resistance transition temperature is $T_c^{\text{zero}} = 6.7$ K. The inset in Fig. 1(b) shows the temperature dependence of the magnetization under a field of 1 Oe. The magnetization was measured on one sample taken from the same batch. The onset transition temperature of the magnetization is about 7.1 K, which is very close to the temperature of the middle transition point of resistivity displayed in Fig. 1(b).

Figures 2(a) and 2(b) show the longitudinal resistivity $\rho_{xx} - H$ and Hall resistivity $\rho_{xy} - H$ as a function of magnetic field for the Bi2201 sample. The Hall resistivity at 20 K changes linearly with the magnetic field. The Hall resistivity at 10 K exhibits a certain bending under low magnetic fields, indicating that the flux motion starts to involve. Below about 9 K, the Hall resistivity shows a sign reversal in a certain field region. With further decrease of temperature, the amplitude of negative Hall resistivity increases and reaches the maximum

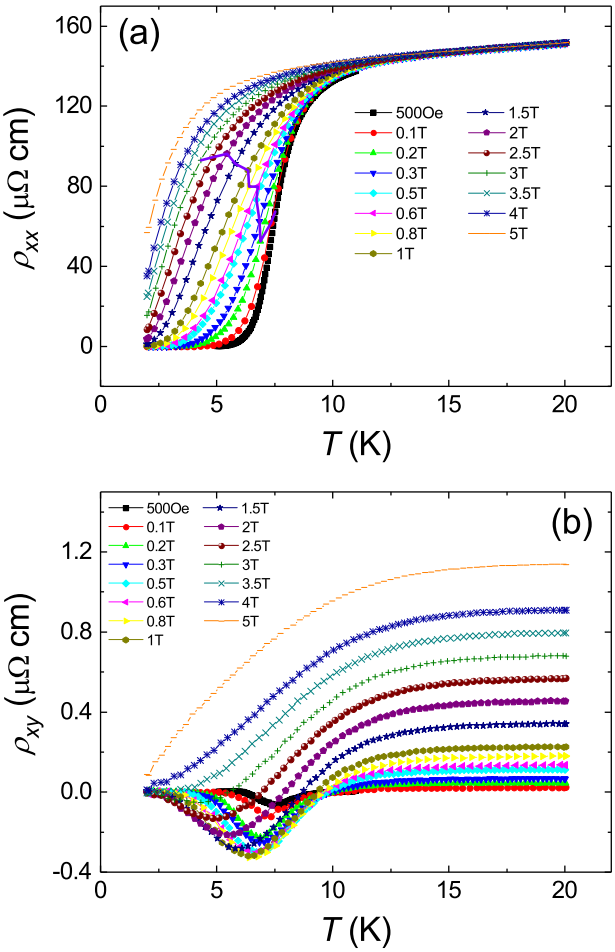

FIG. 3. (a) Longitudinal resistivity of the Bi2201 sample as a function of temperature under different magnetic fields. The magnetic field ranges from 0.05 T to 5 T. The dark purple thick solid line represents the positions of the maximum negative Hall resistivity in Figure 3(b). (b) Temperature dependence of the Hall resistivity under different magnetic fields.

at 6 K or 7 K. With the further decrease of temperature, the amplitude of negative Hall resistivity will decrease. The inset in Fig. 2(b) displays the Hall resistivity at 1.6 K and 2 K. The Hall resistivity at 1.6 K still exhibits a slight sign reversal, although the signal becomes already very small. As shown in Fig. 2(b), the negative Hall resistivity of Bi2201 usually appears at moderate magnetic fields and the maximum value of AHE appears at temperatures near T_c^{zero}. For example, the strongest AHE appears at about $6 \sim 7$ K which is close to $T_c^{\text{zero}} \approx 6.7$ K. This behavior has also been observed in $YBa_2Cu_3O_7$ [7]. In Fig. 2(a), we use a dark purple dashed line to highlight the positions where the largest Hall reversal signal appears. Figures 3(a) and 3(b) display the temperature dependence of the longitudinal resistivity and Hall resistivity of the Bi2201 sample at some fixed magnetic fields. The Hall resistivity data in Fig. 3(b) and the Hall resistivity data in Fig. 2(b) can be mutually verified. As displayed in Fig. 3(b), the Hall resistivity in Bi2201 shows a single sign reversal, which is very different from the double sign reversal in Bi2212 [1,40]. Again in Fig. 3(a), we use a dark purple, thick solid line to highlight the positions where the largest Hall reversal signal appears. One can see that the largest Hall reversal signal appears in the middle of the transition.

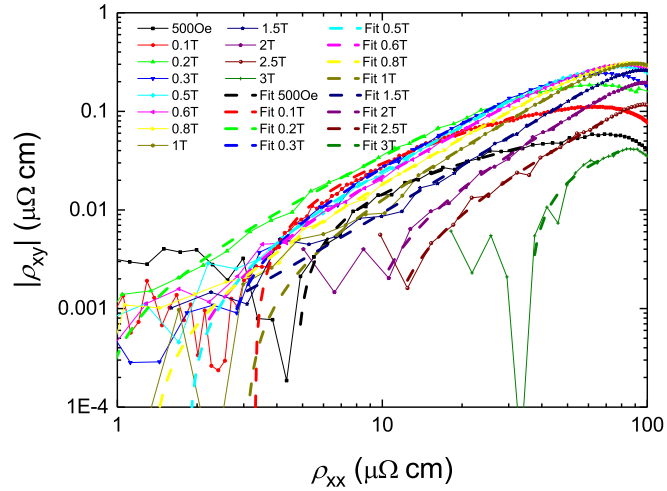

FIG. 4. Scaling behavior between the Hall resistivity ρ_{xy} and longitudinal resistivity ρ_{xx} under the magnetic field between 0.05 T and 3 T. The symbols represent the absolute value of the Hall resistivity ρ_{xy}. The dashed lines are fits of the $|\rho_{xy}|$ data using the formula $|\rho_{xy}| = A\rho_{xx}^b(\rho_{xx} + c)$, where A, b, and c are the fitting parameters. This figure displays the region where the scaling behavior may appear.

B. Scaling behavior

The scaling behavior $\rho_{xy} = A\rho_{xx}^{\beta}$ with $1.5 < \beta < 2$ was argued to appear in the region for the Hall reversal effect in some superconductors [2,5,11,13,37]. Figure 4 displays the scaling behavior between the absolute value of the Hall resistivity ρ_{xy} and the longitudinal resistivity ρ_{xx} under different magnetic fields. This figure shows the region where the scaling behavior may occur. In the double logarithmic plot, it seems that the data do not exhibit as a linear line, but show some curved feature. Thus, practically, our data show a deviation from the simple scaling law. We then fit the data of $|\rho_{xy}|$ versus ρ_{xx} via the formula $|\rho_{xy}| = A\rho_{xx}^b(\rho_{xx} + c)$, where A, b, and c are the fitting parameters. The parameter b derived from fitting is displayed in Table I. The parameter b increases from 0.282 to 0.643 when the magnetic field increases from 0.2 T to 1.5 T. The parameter b decreases from 0.643 to 0.349 when the magnetic field increases from 1.5 T to 2.5 T. Here, we

TABLE I. Parameter b, related β, and parameter c in the fitting results.

	0.05 T	0.1 T	0.2 T	0.3 T	0.5 T	0.6 T
b	−0.494	−0.306	0.282	0.285	0.369	0.407
$\beta \approx b + 1$	0.506	0.694	1.282	1.285	1.369	1.407
c	−4.730	−0.0292	−0.8307	−2.417	−1.846	−1.669
	0.8 T	1 T	1.5 T	2 T	2.5 T	
b	0.448	0.456	0.643	0.401	0.349	
$\beta \approx b + 1$	1.448	1.456	1.643	1.401	1.349	
c	−1.331	−3.040	0.5535	−8.259	−9.831	

do not consider the data with a magnetic field of 3 T, since the data at 3 T has a small negative Hall resistivity and relatively large longitudinal resistivity. We can see that the double logarithmic plot of $|\rho_{xy}|$ versus ρ_{xx} shows a certain linearity in the small dissipation region when the magnetic field ranges from 0.5 T to 2.5 T, but clearly a simple scaling law $\rho_{xy} = A\rho_{xx}^{\beta}$ is not obeyed in a wide region of ρ_{xx}. We also put the scaling exponent $\beta \approx b + 1$ and parameter c in the table. We can see that the values of c under different magnetic fields are one or two orders of magnitude smaller than ρ_{xx} (except for 3 T). Ignoring the influence of c, we believe that the scaling exponent β is approximately equal to $b + 1$. The scaling exponent β increases from 1.282 to 1.643, when the magnetic field increases from 0.2 T to 1.5 T. The scaling exponent β decreases from 1.643 to 1.349, when the magnetic field increases from 1.5 T to 2.5 T. One can see that β is generally smaller than 2. This means that the $|\rho_{xy}|$ with magnetic field ranging from 0.5 T to 2.5 T satisfies the so-called scaling behavior with $1.349 < \beta < 1.643$. The simple scaling law between $|\rho_{xy}|$ and ρ_{xx} may be satisfied in the case of weak pinning [41]. The strong pinning will destroy this scaling behavior [41]. The $|\rho_{xy}|$ with magnetic field between 0.05 T and 0.5 T corresponds to the small dissipation region of ρ_{xx}, corresponding to strong pinning, thus it doesn't exhibit the scaling behavior. Therefore, our Bi2201 sample does not fully satisfy this scaling behavior, but a modified equation $|\rho_{xy}| = A\rho_{xx}^{b}(\rho_{xx} + c)$ seems to fit the data better. Kang *et al.* also obtained the scaling behavior with $\beta = 1.5$ by adding columnar defects in the $YBa_2Cu_3O_7$ sample [13]. Our sample is relatively clean, which should be different from theirs, but disorders or enhanced pinning strength will change the anomalous Hall effect and also the scaling exponent.

C. Phase diagram of Hall resistance

Figure 5 displays the phase diagram of the Hall resistivity obtained from the Hall resistivity displayed in Fig. 2(b). In Fig. 5, the red area represents the positive Hall resistivity region, the blue area denotes the negative Hall resistivity region, and the white areas represent the zero Hall resistivity regions. The black square symbols displayed in Fig. 5 represent the locus $\rho_{xy}(B, T) = 0$ obtained from the $\rho_{xy} - H$ data. The cyan triangle symbols denote the locus $\rho_{xy}(B, T) = 0$ obtained from the $\rho_{xy} - T$ data. The green solid line denotes the irreversible field H_{irr} determined from the resistivity ρ_{xx}^{irr}=1%$\rho_{xx}^{n}(T)$, where $\rho_{xx}^{n}(T)$ is the linear extrapolation of the normal state resistivity measured between 10 and 20 K under a high magnetic field of 15 T. We can see that the locus $\rho_{xy}(B, T) = 0$ in the low temperature region does not decrease, which is completely different from the situation in Bi2212 [40]. It is not clear why the Hall resistance of Bi2201 has a single sign reversal, while the Hall resistance of Bi2212 has a double sign reversal [40]. Superconductors with double sign reversal seem to have relatively high T_c. It seems that superconductors with wider vortex liquid regions are more likely to show the double sign reversal of Hall resistance. The red dashed line in Fig. 5 displays the fitting result of the locus $\rho_{xy}(B, T) = 0$ obtained from the $\rho_{xy} - H$ data, via the theory proposed by Feigel'man *et al.* [30]. In Fig. 5, the locus $\rho_{xy}(B, T) = 0$ obtained from the $\rho_{xy} - H$ data is very close to that obtained from the $\rho_{xy} - T$ data, so we only need to fit the former instead of both.

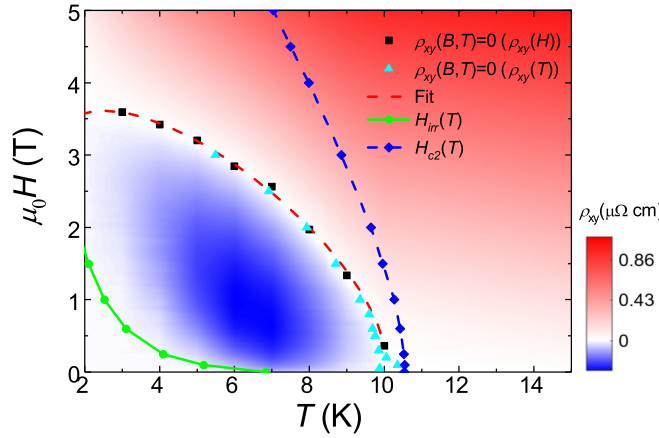

FIG. 5. (a) Phase diagram of the Hall resistivity as a function of magnetic field. The color intensity reflects the Hall resistivity, as marked by the color bar. The black square symbols show the locus $\rho_{xy}(B, T) = 0$ obtained from the $\rho_{xy} - H$ data. The cyan triangle symbols denote the locus $\rho_{xy}(B, T) = 0$ obtained from the $\rho_{xy} - T$ data. The red dashed line displays the fitting result of the locus $\rho_{xy}(B, T) = 0$ obtained from the $\rho_{xy} - H$ data, via Eq. (6). The green solid line denotes the irreversible field $H_{\rm irr}$. The blue diamond symbols represent the upper critical field H_{c2} of Bi2201 determined from the resistivity $\rho_{xx}^{\rm upp}$=95%$\rho_{xx}^{n}(T)$, where $\rho_{xx}^{n}(T)$ is the linear extrapolation of the normal state resistivity to lower temperatures. It is interesting to note that the curve corresponding to $\rho_{xy}(B, T) = 0$ shows a negative curvature in whole temperature region as the $H_{c2}(T)$ in high temperature region, but the latter shows a divergence in low temperature region [39]. The lines in the figure are guides to the eyes.

In the present paper, we use the model of Feigel'man *et al.* [30] to analyze our data. Starting from the basic equation of vortex motion and considering topological contribution and normal excitation, they attributed the AHE to the excess charge in the vortex core [30]. In their model, the Hall conductivity can be written as [30]

$$\sigma_{xy} = \frac{\Delta^2 n_0 e}{E_F^2 B}\left[g\frac{(\tau\Delta)^2}{\hbar^2} - \mathrm{sgn}(\delta n)\right] + \sigma_{xy}^{n}(1-g). \quad (1)$$

Here, δn is related to the excess charge in the vortex core, that is, the charge carrier density in the vortex core minus the charge carrier density outside the vortex core. n_0 is the normal carrier density inside the vortex core, g represents the superconducting part of the carrier, and σ_{xy}^{n} denotes the Hall conductivity of the normal state. This formula is now written in the units of the International Standard System. Using the two-fluid model [42], we can simplify $g(T)$ and get

$$g(T) = 1 - (T/T_c)^2. \quad (2)$$

The Hall conductivity of the normal state should be proportional to magnetic field, and we can get

$$\sigma_{xy}^{n} = S_{xy}^{n} B. \quad (3)$$

Here, S_{xy}^{n} should be positive and independent of magnetic field B. To get the sign-reversal locus, $\rho_{xy}(B, T) = 0$, we should substitute Eq. (3) into Eq. (1) and make $\mathrm{sgn}(\delta n) = 1$ as well

as $\sigma_{xy} = 0$. Therefore, we can get the relation for the boundary of the Hall reversal effect, namely, $\rho_{xy}(B, T) = 0$, which reads

$$B^2 = \left(\frac{\Delta}{E_F}\right)^2 \frac{n_0 e}{S_{xy}^n} \frac{[1 - (\Delta\tau/\hbar)^2 g]}{1 - g}. \tag{4}$$

In Eq. (4), the relaxation time τ, T_c^{onset}, and the carrier density n_0 are the fitting parameters. $\Delta(T)$ and S_{xy}^n should depend on temperature. We can simply write $\Delta(T)$ as [42]

$$\Delta(T) = 1.74\Delta_0\left(1 - \frac{T}{T_c}\right)^{1/2}. \tag{5}$$

Here, $\Delta(T)$ is considered to be independent of the magnetic field, since the magnetic fields where the negative Hall resistance occurs are much lower than the upper critical field H_{c2}. For the convenience of fitting, we write Eq. (4) in the following form:

$$B = f\left(1 - \frac{T}{T_c}\right)^{1/2} \sqrt{\frac{T_c^2 - j(1 - T/T_c)(T_c^2 - T^2)}{T}}. \tag{6}$$

Here, $f = \sqrt{(1.74\Delta_0/E_F)^2 n_0 e(1/a)}$, $T_c = T_c^{\text{onset}}$ and $j = (\Delta\tau/\hbar)^2$ are the indirect fitting parameters. In this formula, we assume $S_{xy}^n = a/T + d$. We use this formula to fit the locus $\rho_{xy}(B, T) = 0$ and compare the results with Eq. (4). In our Bi2201 sample, we can take roughly $\Delta(0) \approx 2$ meV as determined from the Bi2201 sample [43] with the similar T_c. Then, we can obtain $\tau = 3.38 \times 10^{-13}$ s by fitting the locus $\rho_{xy}(B, T) = 0$ obtained from the $\rho_{xy} - H$ data in Fig. 5 with Eq. (6).

Figure 6(a) shows the Hall conductivity of Bi2201 at different temperatures. Here, we use $\sigma_{xy} = \rho_{xy}/\rho_{xx}^2$ to get the Hall conductivity σ_{xy}. We fit the Hall conductivity σ_{xy} linearly and get S_{xy}^n. Figure 6(b) displays the slope of the Hall conductivity in the normal state. Then we fit S_{xy}^n in the normal state using the formula $S_{xy}^n = a/T + d$, and get $a = 16914$, $d = 70.1$. We assume that this $S_{xy}^n \propto 1/T$ dependence can be extrapolated to low temperatures from the normal state. We can get $\Delta(0)/E_F = 0.01$, since the superconducting gap $\Delta(0)$ of cuprates is often one or two orders of magnitude smaller than E_F [44]. Then we can fit the locus $\rho_{xy}(B, T) = 0$ obtained from the $\rho_{xy} - H$ data displayed in Fig. 5 via Eq. (6) and get $T_c^{\text{onset}} = 10.07$ K and $n_0 = 1.76 \times 10^{27}$ m^{-3}. The parameter $T_c^{\text{onset}} = 10.07$ K conforms to the situation in our Bi2201, and the parameter $n_0 = 1.76 \times 10^{27}$ m^{-3} is close to the widely accepted value in cuprates which is $n_0 \approx 10^{27}$ m^{-3} [45]. In Fig. 5, the Hall resistivity of Bi2201 does not show a second sign reversal at low temperatures, since at low temperatures the system enters the irreversible regime. Generally speaking, we can fit our data in Fig. 5 very well via Eq. (6) and the related fitting parameters conform to the generally accepted values. We can see that the data can be nicely fitted by the theoretical model. Therefore, we believe that the model of Feigel'man *et al.* [30] can capture the major physics of AHE in the sample Bi2201.

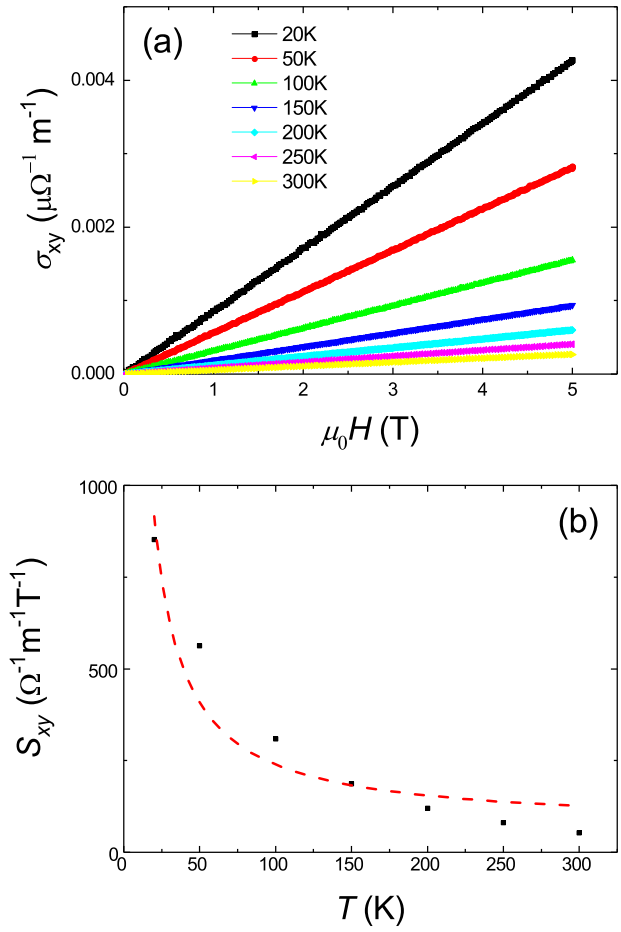

FIG. 6. (a) The Hall conductivity of Bi2201 at different temperatures. (b) The slope of the Hall conductivity as a function of temperature. The red dashed line is the fit of S_{xy}^n using the formula $S_{xy}^n = a/T + d$, where a and d are fitting parameters.

III. CONCLUSION

In conclusion, we have measured the longitudinal and transverse Hall resistivity of the Bi2201 single crystal with a well shaped structure of Hall bar. Anomalous Hall effect has been observed in the flux flow region. The maximum signal of AHE effect for each fixed magnetic field or temperature appears roughly on the half way of the transition. The supposed scaling law of $\rho_{xy} = A\rho_{xx}^{\beta}$ with $1.5 < \beta < 2$ is not fully satisfied. Our Bi2201 shows a single sign reversal instead of the double sign reversal. We obtained the phase diagram concerning the Hall reversal effect and found that the locus of the boundary corresponding to $\rho_{xy}(B, T) = 0$ can be nicely fitted by the theoretical model of Feigel'man *et al.* [30].

ACKNOWLEDGMENTS

This work was supported by the National Natural Science Foundation of China (Grants No. 11927809, No. NSFC-DFG12061131001, and No. 62288101), the National Key R&D Program of China (Grants No. 2022YFA1403200, No. 2023YFA1406103, No. 2018YFA0704201, and No. 2021YFA0718802), and the Strategic Priority Research Program of Chinese Academy of Sciences (Grant No. XDB25000000).

[1] Y. Iye, S. Nakamura, and T. Tamegai, Physica C **159**, 616 (1989).
[2] A. V. Samoilov, Phys. Rev. Lett. **71**, 617 (1993).
[3] S. J. Hagen, C. J. Lobb, R. L. Greene, and M. Eddy, Phys. Rev. B **43**, 6246 (1991).
[4] A. V. Samoilov, Z. G. Ivanov, and L.-G. Johansson, Phys. Rev. B **49**, 3667 (1994).
[5] R. C. Budhani, S. H. Liou, and Z. X. Cai, Phys. Rev. Lett. **71**, 621 (1993).
[6] A. Dascoulidou, M. Galffy, C. Hohn, N. Knauf, and A. Freimuth, Physica C **201**, 202 (1992).
[7] T. R. Chien, T. W. Jing, N. P. Ong, and Z. Z. Wang, Phys. Rev. Lett. **66**, 3075 (1991).
[8] S. J. Hagen, C. J. Lobb, R. L. Greene, M. G. Forrester, and J. H. Kang, Phys. Rev. B **41**, 11630 (1990).
[9] M. N. Kuncher, D. K. Christen, C. E. Klabunde, and J. M. Phillips, Phys. Rev. Lett. **72**, 2259 (1994).
[10] J. P. Rice, N. Rigakis, D. M. Ginsberg, and J. M. Mochel, Phys. Rev. B **46**, 11050 (1992).
[11] J. Luo, T. P. Orlando, J. M. Graybeal, X. D. Wu, and R. Muenchausen, Phys. Rev. Lett. **68**, 690 (1992).
[12] J. M. Harris, N. P. Ong, and Y. F. Yan, Phys. Rev. Lett. **71**, 1455 (1993).
[13] W. N. Kang, D. H. Kim, S. Y. Shim, J. H. Park, T. S. Hahn, S. S. Choi, W. C. Lee, J. D. Hettinger, K. E. Gray, and B. Glagola, Phys. Rev. Lett. **76**, 2993 (1996).
[14] W. N. Kang, S. H. Yun, J. Z. Wu, and D. H. Kim, Phys. Rev. B **55**, 621 (1997).
[15] T. Nagaoka, Y. Matsuda, H. Obara, A. Sawa, T. Terashima, I. Chong, M. Takano, and M. Suzuki, Phys. Rev. Lett. **80**, 3594 (1998).
[16] A. W. Smith, T. W. Clinton, C. C. Tsuei, and C. J. Lobb, Phys. Rev. B **49**, 12927 (1994).
[17] S. Bhattacharya, M. J. Higgins, and T. V. Ramakrishnan, Phys. Rev. Lett. **73**, 1699 (1994).
[18] S. J. Hagen, A. W. Smith, M. Rajeswari, J. L. Peng, Z. Y. Li, R. L. Greene, S. N. Mao, X. X. Xi, S. Bhattacharya, Q. Li, and C. J. Lobb, Phys. Rev. B **47**, 1064 (1993).
[19] L. M. Wang, U.-C. Sou, H. C. Yang, L. J. Chang, C.-M. Cheng, K.-D. Tsuei, Y. Su, T. Wolf, and P. Adelmann, Phys. Rev. B **83**, 134506 (2011).
[20] I. Tsukada, M. Hanawa, S. Komiya, T. Akiike, R. Tanaka, Y. Imai, and A. Maeda, Phys. Rev. B **81**, 054515 (2010).
[21] J. Bardeen and M. J. Stephen, Phys. Rev. **140**, A1197 (1965).
[22] P. Ao, J. Low Temp. Phys. **89**, 543 (1992).
[23] A. T. Dorsey, Phys. Rev. B **46**, 8376 (1992).
[24] J. Friedel, P. G. de Gennes, and J. Matricon, Appl. Phys. Lett. **2**, 119 (1963).
[25] P. Nozières and W. F. Vinen, Philos. Mag. **14**, 667 (1966).
[26] P. Ao and D. J. Thouless, Phys. Rev. Lett. **70**, 2158 (1993).
[27] Z. D. Wang and C. S. Ting, Phys. Rev. Lett. **67**, 3618 (1991).
[28] Z. D. Wang, J. Dong, and C. S. Ting, Phys. Rev. Lett. **72**, 3875 (1994).
[29] V. M. Vinokur, V. B. Geshkenbein, M. V. Feigel'man, and G. Blatter, Phys. Rev. Lett. **71**, 1242 (1993).
[30] M. V. Feigel'man, V. B. Geshkenbein, A. I. Larkin, and V. M. Vinokur, JETP Lett. **62**, 834 (1995).
[31] A. G. Aronov, S. Hikami, and A. I. Larkin, Phys. Rev. B **51**, 3880 (1995).
[32] S. Ullah and A. T. Dorsey, Phys. Rev. B **44**, 262 (1991).
[33] K. Michaeli, K. S. Tikhonov, and A. M. Finkelstein, Phys. Rev. B **86**, 014515 (2012).
[34] P. Ao, J. Phys.: Condens. Matter **10**, L677 (1998).
[35] A. Freimuth, C. Hohn, and M. Galffy, Phys. Rev. B **44**, 10396(R) (1991).
[36] J. L. Chen and T. J. Yang, Phys. Rev. B **50**, 4064 (1994).
[37] A. V. Samoilov, A. Legris, F. Rullier-Albenque, P. Lejay, S. Bouffard, Z. G. Ivanov, and L.-G. Johansson, Phys. Rev. Lett. **74**, 2351 (1995).
[38] H. Luo, L. Fang, G. Mu, and H.-H. Wen, J. Cryst. Growth **305**, 222 (2007).
[39] Q. Zang, Z. Zhu, Z. Xu, S. Qi, H. Ji, Y. Li, J. Wang, H. Luo, H.-B. Wang, and H.-H. Wen, Sci. China Phys. Mech. Astron. **66**, 237412 (2023).
[40] S. Y. Frank Zhao, N. Poccia, M. G. Panetta, C. Yu, J. W. Johnson, H. Yoo, R. Zhong, G. D. Gu, K. Watanabe, T. Taniguchi, S. V. Postolova, V. M. Vinokur, and P. Kim, Phys. Rev. Lett. **122**, 247001 (2019).
[41] N. B. Kopnin and V. M. Vinokur, Phys. Rev. Lett. **83**, 4864 (1999).
[42] M. Tinkham, *Introduction to Superconductivity*, 2nd ed. (Dover Publications, New York, 2004).
[43] J. M. Harris, P. J. White, Z.-X. Shen, H. Ikeda, R. Yoshizaki, H. Eisaki, S. Uchida, W. D. Si, J. W. Xiong, Z.-X. Zhao, and D. S. Dessau, Phys. Rev. Lett. **79**, 143 (1997).
[44] A. K. Saxena, *High-Temperature Superconductors* (Springer, Berlin/Heidelberg, 2012).
[45] A. T. Bollinger and I. Božović, Supercond. Sci. Technol. **29**, 103001 (2016).